Computers and Chemical Engineering 152 (2021) 107391

Contents lists available at ScienceDirect

Computers and Chemical Engineering

journal homepage: www.elsevier.com/locate/compchemeng

Multi-scale fluid dynamics simulation based on MP-PIC-PBE method for PMMA suspension polymerization

Shin Hyuk Kim, Ph. D[a], Jay H. Lee[a,*], Richard D. Braatz[b]

[a] Department of Chemical and Biomolecular Engineering, Korea Advanced Institute of Science and Technology, 291 Daehak-Ro, Yuseong-Gu, Daejeon, 34141, Republic of Korea
[b] Massachusetts Institute of Technology, 77 Massachusetts Avenue, Cambridge, MA 02139, USA

ARTICLE INFO

Article history:
Received 2 March 2021
Revised 25 May 2021
Accepted 30 May 2021
Available online 2 June 2021

Keywords:
Computational fluid dynamics
Dense particulate flow
Suspension polymerization
Population balance equation
Particle breakage

ABSTRACT

This research presents an advanced multi-scale computational fluid dynamics (CFD) model based on the 'multi-phase particle-in-cell coupled with the population balance equation (MP-PIC-PBE)' method to predict the stationary continuous stirred tank reactor for methyl methacrylate suspension polymerization. The developed CFD model can realistically simulate the flow patterns of the free-flowing particles and the continuous carrier phase based on the Euler-Lagrangian frame and can track the change in particle size based on PBE. In particular, the model can predict the polymer properties by free-radical polymerization in a parcel through the method of moment equations. To validate the suggested CFD model, the simulation results are compared with the reported experimental data in the literature. Various case-studies are then conducted to investigate the effect of different blade angles (pitched blade angles of 30°, 45°, and 60°) of the impeller on the mixing, the particle size change, particulate flow pattern, and polymer properties. The simulation results demonstrate the phenomena that the low-density particles rise in the larger density solvent by buoyancy and that the higher the blade angle, the smaller the resulting particles due to a higher rate of breakage. It is also found that the particulate flow is well mixed with a 45° blade angle.

1. Introduction

Suspension polymerization is a process of producing free-flowing polymer particles using two immiscible liquid phases. The process first creates a suspension of monomer droplets within a continuous liquid phase – typically water – after which polymerization occurs in the droplets to form solid polymer beads. This approach makes it easy to remove the heat of reaction generated in the droplets and is suitable for large-scale industrial polymerizers because there is limited increase in viscosity (Hungenberg & Wulkow, 2018). This situation is in contrast to bulk polymerization in which the viscosity increases by several orders of magnitude during the polymerization, causing operational problems at a large scale. The polymer beads resulting from suspension polymerization are nearly perfect spheres and are easy to transport, store, and feed to polymer extrusion processes to make products in the form of fibers, films, textiles, etc. (Dowding & Vincent, 2000).

The size distribution of the free-flowing droplets has a direct effect on the size distribution of the resulting polymer particles, which also directly affects the polymer's molecular weight distribution and thus quality of the polymer products. The size of particles is determined by the turbulence resistance and the dynamic equilibrium of the coalescence by surface tension and adhesion force (Ramkrishna, 2000). Therefore, if the fluid dynamics which shapes the particle size distribution (PSD), both initially and as the polymerization progresses, can be controlled, it would be possible to control the properties of the polymer product beyond what is currently achievable by the control of temperature and feed compositions. However, there is still a lack of understandings on the relationship between the size of dispersed particles and the fluid dynamics (E. H. Hukkanen, 2004). Studies in the past have not been able to accurately predict particle size and molecular weight distribution simultaneously since they could not interpret the precise flow pattern inside the reactor (Barkanyi & Nemeth, 2015; Barkanyi et al., 2013; Okullo et al., 2017). Although the combination of computational fluid dynamics (CFD) and population balance equations (PBE) is the state of the art (Xie & Luo, 2017), there are limitations such as the expensive computational cost and the incorrect particle motion (Rigopoulos, 2010). As such, the

* Corresponding author.
E-mail addresses: kimshinhyuk@kaist.ac.kr (S.H. Kim), jayhlee@kaist.ac.kr (J.H. Lee), braatz@mit.edu (R.D. Braatz).

https://doi.org/10.1016/j.compchemeng.2021.107391
0098-1354/

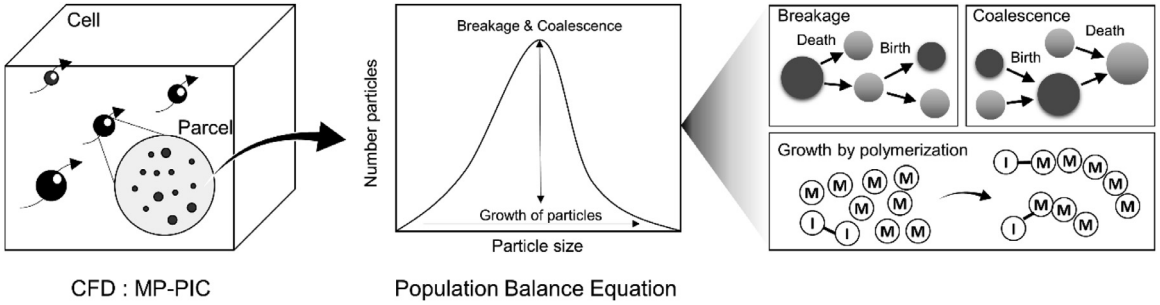

Fig. 1. Schematic diagram of the MP-PIC-PBE for suspension polymerization

development of mathematical models and numerical methods to accurately predict the fluid dynamics and particle size and molecular weight distributions in suspension polymerization systems is still in progress.

To this end, this research is intended to advance the state of the art by developing a multiscale mathematical model and simulator that can predict both the PSD and the average molecular weight simultaneously, taking the detailed fluid dynamics rigorously into account. The model, developed using the recently proposed multiphase particle-in-cell coupled with population balance equation (MP-PIC-PBE) method (Kim et al., 2020), graphically simulates the suspended multiphase flow based on the Euler-Lagrangian frame which presents not only the lift and drag forces between the particle phase and the continuous solvent phase but also the inter-particles collision and damping effects. In addition, the micro-scale particle changes are predicted through the implementation of the droplet growth by polymerization and droplet breakage by turbulence energy dissipation. The additional polymerization modeling computes the various polymer properties of individual droplets such as the average molecular weight, and the polydispersity index (PD).

A continuous stirred-tank reactor of poly methyl methacrylate (PMMA) suspension polymerization, previously studied in (Roudsari et al., 2013), is simulated for validation and a case study. The simulations are validated with research results in the literature (E. H. Hukkanen, 2004; E. J. Hukkanen & Braatz, 2005a, 2005b; E. J. Hukkanen et al., 2007), and the interaction between turbulence energy dissipation rate and particle breakage (Hsia, 1981) is clearly elucidated in the case study. In particular, the effect of different blade angles of the impeller on particle size changes is investigated.

2. MP-PIC-PBE for suspension polymerization

The MP-PIC method is widely used to analyze oil and gas particulate processes such as a fluidized bed, and a hydrocyclone separator (Razmi et al., 2019; Thapa et al., 2016). These examples have demonstrated the ability of the MP-PIC method to predict the flow patterns of multi-phase fluids when a liquid or gas carrier phase and the particulate phase are mixed. However, a limitation of the MP-PIC method is that it is difficult to predict changes in particle size due to reactions and external forces. The MP-PIC-PBE method have been developed to efficiently and accurately predict the particle size change by tracking the particle size distribution inside a parcel (Kim et al., 2020).

In this study, the MP-PIC-PBE method is modified to address the suspension polymerization phenomena as shown in Figure 1. The newly built model is able to predict the particulate multiphase fluid dynamics based on the MP-PIC method (Snider, 2001; Snider et al., 1997), and reflect the change of particle size in parcels with respect to the fluid flow based on the PBE. A parcel refers to a collection of particles having a same flow pattern, and it is assumed that the particles inside a parcel can increase or decrease in size due to chemical changes and particle-to-particle interactions. In suspension polymerization, changes in particle size are accounted for by a set of phenomena including breakage, coalescence, and growth. The turbulent energy of flow causes breakage, the inter-particle collision affects coalescence, and the polymerization results in particle growth.

2.1. Continuous fluid phase

The mass, momentum, and energy governing equations for the continuous phase, with the assumption of incompressible flow, are expressed by

Mass equation

$$\frac{\partial \theta_f}{\partial t} + \nabla \cdot \left(\theta_f u_f\right) = 0 \tag{1}$$

Momentum equation

$$\frac{\partial \left(\theta_f u_f\right)}{\partial t} + \nabla \cdot \left(\theta_f u_f u_f\right) + \frac{1}{\rho_f}\nabla \cdot \tau = -\frac{1}{\rho_f}\nabla \mathrm{P} + \theta_f g - \frac{\mathrm{F}}{\rho_f} \tag{2}$$

Energy equation

$$\frac{\partial \left(\theta_f h_f\right)}{\partial t} + \nabla \cdot \left(\theta_f u_f h_f\right) + \frac{\partial \left(\theta_f K_f\right)}{\partial t} + \nabla \cdot \left(\theta_f u_f K_f\right) - \frac{\theta_f}{\rho_f}\frac{\partial \mathrm{P}}{\partial t}$$
$$= \frac{1}{\rho_f}\nabla \cdot \theta_f\left[k_{eff}\nabla \mathrm{T} + \left(\overline{\overline{\tau}}_{eff} \cdot u_f\right)\right] + \theta_f g \cdot u_f \tag{3}$$

where θ_f is the fluid volume fraction, ρ_f is the fluid density, u_f is the fluid velocity, τ is the shear stress by viscous and turbulent flow, P is the system pressure, g is the gravitational acceleration, F is the interphase momentum transfer which includes the viscous drag between particles as well as between the particulate phase and the fluid phase, h_f is the fluid enthalpy, $K_f = |u_f|^2/2$ is the kinetic energy, k_{eff} is the fluid thermal conductivity, T is the system temperature, and $\overline{\overline{\tau}}_{eff} \cdot u_f$ is the mechanical source.

2.2. Particulate phase

The particulate phase equations from applying MP-PIC are given by (Snider, 2001)

Particle distribution function

$$\frac{\partial f}{\partial t} + \nabla \cdot (f v_p) + \nabla_{v_p} \cdot (fA) = 0 \tag{4}$$

Particle acceleration

$$\frac{\partial v_p}{\partial t} = \mathrm{A} = F_D + F_L - \frac{1}{\rho_p}\nabla \mathrm{P} + g - \frac{1}{\theta_p \rho_p}\nabla \tau_p \tag{5}$$

Particle drag force

$$F_D = \mathrm{C}_d \frac{3}{8}\frac{\rho_f}{\rho_p}\frac{\left|u_f - v_p\right|}{r_p}\left(u_f - v_p\right) \tag{6}$$

where

$$C_d = \frac{24}{\mathrm{Re}}\theta_f^{-2.65}\left(1 + 0.5\mathrm{Re}^{0.687}\right); \quad if\ \mathrm{Re} < 1000$$

$$C_d = 0.44\ \theta_f^{-2.65}; \qquad if\ \mathrm{Re} \geq 1000$$

$$\mathrm{Re} = \frac{2\rho_f |u_f - v_p| r_p}{\mu_f}$$

Particle shear lift force

$$F_L = 6.46\rho_f \nu^{\frac{1}{2}} r_p \left(u_f - v_p\right)\left|\frac{du_f}{dy}\right|^2 sign\left(\frac{du_f}{dy}\right) \tag{7}$$

Isotropic interparticle stress

$$\tau_p = \frac{P_s \theta_p{}^{\beta}}{\max\{\theta_{cp} - \theta_p,\ \varepsilon(1-\theta_p)\}} \tag{8}$$

Particle volume fraction

$$\theta_p = \iint f \frac{m}{\rho_p} dm dv \tag{9}$$

Liquid volume fraction

$$\theta_f + \theta_p = 1 \tag{10}$$

Interphase momentum transfer function

$$\mathrm{F} = \iint fm\left[F_D + F_L - \frac{1}{\rho_p}\nabla \mathrm{P}\right] dm\ dv \tag{11}$$

where f is the particle distribution function in the Euler grid, v_p is the discrete particle velocity, A is the discrete particle acceleration, F_D is the particle drag function, ρ_p is the particle density which is a mixture density of polymer and monomer in a parcel, F_L is the particle shear lift function, C_d is the drag coefficient, r_p is the particle mean radius, τ_p is the interparticle stress, P_s is a constant in units of pressure, θ_p and θ_{cp} are the particle volume fraction and its maximum, β is a constant whose value is recommended between 2 and 5, ε is a small number on the order of $10^{-7,}$ and m is the total mass of the particles in a parcel (Snider et al., 1997).

2.3. Population balance equations in a parcel

During suspension polymerization in a CSTR, the particles collide with each other to merge or split, and also grow by polymerization. By such phenomena, the distribution of population in a parcel is changed through growth, birth, and death of particles as described in Eqs. (12)–(14):

$$\frac{\partial N_j}{\partial t} = -\sum_j \frac{\partial\left[G(x,T)N_j\right]}{\partial r_j} + B\left(N_j, T\right) - D\left(N_j, T\right) \tag{12}$$

$$B\left(N_j, T\right) = \int_j^{\infty} \beta\left(N_j, r\right) b(r) \upsilon(r) N_j\ dr + \frac{1}{2}\int_0^j c\left[N_{\left(j^3 - r^3\right)^{1/3}}, r\right] N_{\left(j^3 - r^3\right)^{1/3}} N_j\ dr \tag{13}$$

$$D\left(N_j, T\right) = b\left(N_j\right) N_j + N_j \int_0^{\infty} c\left(N_j,\ r\right) N_r\ dr \tag{14}$$

where N_j is the particle number density within a parcel, $G(x,T)$ is the growth rate, r_j is the particle's internal coordinate, $B(N_j,T)$ is the birth rate of particles, $D(N_j,T)$ is the death rate of particles, r is the dimension of particle distribution, $\beta(N_j,\ r)$ is the size distribution of daughter particles formed from breakage of a droplet, $b(r)$ is the breakage frequency, $\upsilon(r)$ is the number of dispersed fluid entities formed from breakage of a particle, and $c(N_j,\ r)$ is the collision frequency. The total mass of a parcel and the average particle size can be calculated by

$$N_{w,j} = \frac{\pi \rho_p}{6} \int r_p{}^3 N_j dr \tag{15}$$

$$m = V_{cell} \sum_j N_{w,j} \tag{16}$$

$$r_p = \frac{D_{32}}{2}$$

where

$$D_{32} = \frac{\sum_j N_{w,j} r_j^3}{\sum_j N_{w,j} r_j^2} \tag{17}$$

and $N_{w,j}$ is the average particle mass per cell volume which is calculated assuming the particles are perfect spheres sized according to the particle size distribution, V_{cell} is the volume of the cell where the particle is positioned, and D_{32} is the volume mean diameter of particles in a parcel.

3. PMMA suspension polymerization

Polymethyl methacrylate (PMMA) is an acrylic polymer derived from acrylic acid and is produced in suspension, solution, and bulk polymerization systems (Ghosh et al., 1998; Kalfas & Ray, 1993; Kalfas et al., 1993; Zhang & Ray, 1997). In general, these systems use anionic polymerization with radical initiation. In this study, suspension polymerization with benzoyl peroxide (BPO) as the initiator and water as the solvent is modeled (Lin & Wang, 1981).

3.1. Free radical polymerization kinetics

The radical polymerization mechanism and kinetics of bulk polymerization used in this study are taken from a previous research done by Hukkanen and coworkers (E. J. Hukkanen et al., 2007). Bulk polymerization with an organic peroxide initiator has the reaction mechanism:

$$I_2 \xrightarrow{k_d} 2I\cdot \qquad r_d = 2f_i k_d [I_2] \qquad \text{initiator decomposition}$$

$$I\cdot + M \xrightarrow{k_i} P_1 \qquad r_i = k_i[M][I\cdot] \qquad \text{initiation}$$

$$P_n + M \xrightarrow{k_p} P_{n+1} \qquad r_p = k_p[M][P_n] \qquad \text{propagation}$$

$$P_n + P_m \xrightarrow{k_{tc}} D_{n+m} \qquad r_{tc} = k_{tc}[P_m][P_n] \qquad \text{termination by combination}$$

where k_d, k_i, k_p, and k_{tc} are the rate constant parameters, f_i is the initiator efficiency parameter, I_2 and $I\cdot$ are the initiator and initiator radical molecule, M is the monomer, P is the live polymer, D is the dead polymer, and m and n represent the chain length.

By assuming a dispersed particle is a well-mixed batch reactor, bulk polymerization is represented to occur inside each particle. The molar balances in a batch reactor are expressed by

Initiator decomposition

$$\frac{1}{V}\frac{\partial([I_2]V)}{\partial t} = -k_d[I_2] \tag{18}$$

Radical concentration

$$\frac{1}{V}\frac{\partial([I\cdot]V)}{\partial t} = -k_i[I\cdot][M] + 2f_i k_d[I_2] \tag{19}$$

Monomer concentration

$$\frac{1}{V}\frac{\partial([\mathrm{M}]V)}{\partial t} = -k_i[I\cdot][M] - k_p[M]\sum_{j=1}^{\infty}\left[P_j\right] \tag{20}$$

Live polymer chains

$$\frac{1}{V}\frac{\partial([P_1]V)}{\partial t} = k_i[I\cdot][M] - k_p[M][P_1] - k_{tc}[P_1]\sum_{j=1}^{\infty}[P_j] \tag{21}$$

Live polymer chains

$$\frac{1}{V}\frac{\partial([P_m]V)}{\partial t} = k_p[M]([P_{m-1}] - [P_m]) - k_{tc}[P_m]\sum_{j=1}^{\infty}[P_j] \quad for\ m = 2, \cdots, n \tag{22}$$

Dead polymer chains

$$\frac{1}{V}\frac{\partial([D_m]V)}{\partial t} = \frac{1}{2}k_{tc}\sum_{j=1}^{m-1}[P_j][P_{m-j}] \quad for\ m = 2, \cdots, n \tag{23}$$

where V is the volume of particle which initially consists of pure monomer.

While the polymerization is in progress, the volume of a particle changes as

$$V = V_0(1 + \varepsilon_{poly}x) \tag{24}$$

$$\varepsilon_{poly} = \frac{\rho_{poly} - \rho_m}{\rho_{poly}} \tag{25}$$

where V_0 is the initial volume of a particle, ε_{poly} is the volume contraction factor, x is the monomer conversion ratio, ρ_{poly} is the polymer density, and ρ_m is the monomer density.

If the lifetime of an initiator radical molecule is extremely short ($<<$ 1 second), the reaction rates of decomposition and initiation can be assumed to be equal as follows:

$$k_i[I\cdot][M] = 2f_ik_d[I_2] \tag{26}$$

With the quasi-steady-state assumption for the concentration of initiator, the governing equation for the initiator radical molecule is

$$\frac{1}{V}\frac{\partial([I_2]V)}{\partial t} = 0 \tag{27}$$

The gel effect is one of auto-acceleration phenomena due to the monomer fraction decreasing during free radical polymerization. This phenomenon limits the monomer diffusion and accelerates the initiation or propagation reaction (Crowley & Choi, 1998). The gel effect is modeled as a function of monomer and polymer ratio (O'Neil et al., 1998), termination rate constant k_{tc}, and propagation rate constant k_p defined as

$$k_{tc} = k_{tc}^0 g_t \tag{28}$$

$$k_p = k_p^0 g_p \tag{29}$$

The gel effect parameters for the termination and propagation are represented by

$$g_t = \begin{cases} 0.10575e^{17.15V_f - 0.01715(T-273.15)} & V_f > V_{f,cr} \\ 0.23\times10^{-5}e^{75V_f} & V_f \le V_{f,cr} \end{cases} \tag{30}$$

$$g_p = \begin{cases} 1 & V_f > V_{f,cr} \\ 0.71\times10^{-4}e^{71.53V_f} & V_f \le V_{f,cr} \end{cases} \tag{31}$$

where V_f is the free volume and $V_{f,cr}$ is the critical free volume.

These are defined by

$$V_f = \phi_m V_{f,m} + \phi_{poly}V_{f,poly}$$

where

$$V_{f,m} = 0.025 + 0.001(T - 167),\quad V_{f,poly} = 0.025 + 0.00048(T - 387) \tag{32}$$

$$V_{f,cr} = 0.1856 - 2.965\times10^{-4}(T - 273.15) \tag{33}$$

where ϕ_m and ϕ_{poly} are the volume fractions of monomer and polymer, and $V_{f,m}$ and $V_{f,poly}$ are the free volumes of monomer and polymer.

Regarding the polymerization kinetics and physical properties used in this study, various constant parameters and functions are used, which are summarized in Table 1.

3.2. Moment equations for free radical polymerization

The method of moments is useful to estimate features of distributed information. In particular, polymer properties with molecular chains of various lengths can be calculated based on average values of the distribution. The polymer moments are defined by

Live polymer moments

$$\lambda_i = \sum_{j=1}^{\infty} j^i[P_j] \tag{34}$$

Dead polymer moments

$$\mu_i = \sum_{j=2}^{\infty} j^i[D_j] \tag{35}$$

where λ_i is the i^{th} moment of live polymer, and μ_i is the i^{th} moment of dead polymer. Note that

$$\sum_{j=1}^{\infty}\frac{\partial}{\partial t}(j^i[P_j]) = \frac{\partial\lambda_i}{\partial t} \text{ for } i = 0,\ 1,\ 2 \tag{36}$$

$$\sum_{j=2}^{\infty}\frac{\partial}{\partial t}(j^i[D_j]) = \frac{\partial\mu_i}{\partial t} \text{ for } i = 0,\ 1,\ 2 \tag{37}$$

By adopting the moment expressions, the infinite dimensional balance equation can be reduced to a finite set of molar balance equations carrying partial information as below: The mass balance equations as introduced in Eqs. (18)–(23) are redefined as

Initiator decomposition

$$\frac{\partial[I_2]}{\partial t} = -\left(k_d + \frac{\varepsilon_{poly}}{1 + \varepsilon_{poly}x}\frac{\partial x}{\partial t}\right)[I_2] \tag{38}$$

Monomer conversion

$$\frac{\partial x}{\partial t} = \frac{2fk_d[I_2](1 + \varepsilon_{poly}x)}{[M_0]} + k_p(1 - x)\lambda_0 \tag{39}$$

0^{th} moment for live polymer

$$\frac{\partial\lambda_0}{\partial t} = 2fk_d[I_2] - k_{tc}\lambda_0^2 - \frac{\varepsilon_{poly}\lambda_0}{1 + \varepsilon_{poly}x}\frac{\partial x}{\partial t} \tag{40}$$

1^{st} moment for live polymer

$$\frac{\partial\lambda_1}{\partial t} = 2fk_d[I_2] + k_p[M]\lambda_0 - k_{tc}\lambda_0\lambda_1 - \frac{\varepsilon_{poly}\lambda_1}{1 + \varepsilon_{poly}x}\frac{\partial x}{\partial t} \tag{41}$$

2^{nd} moment for live polymer

$$\frac{\partial\lambda_2}{\partial t} = 2fk_d[I_2] + k_p[M](2\lambda_1 + \lambda_0) - k_{tc}\lambda_0\lambda_2 - \frac{\varepsilon_{poly}\lambda_2}{1 + \varepsilon_{poly}x}\frac{\partial x}{\partial t} \tag{42}$$

0^{th} moment for dead polymer

$$\frac{\partial\mu_0}{\partial t} = \frac{1}{2}k_{tc}\lambda_0^2 - \frac{\varepsilon_{poly}\mu_0}{1 + \varepsilon_{poly}x}\frac{\partial x}{\partial t} \tag{43}$$

1^{st} moment for dead polymer

$$\frac{\partial\mu_1}{\partial t} = k_{tc}\lambda_0\lambda_1 - \frac{\varepsilon_{poly}\mu_1}{1 + \varepsilon_{poly}x}\frac{\partial x}{\partial t} \tag{44}$$

Table 1
Kinetic parameters and physical constants for PMMA radical polymerization

Parameter	Value	Units	Reference
f_i	1.0	–	(E. H. Hukkanen, 2004)
k_d	$1.7 \times 10^{14}\exp(-3.0 \times 10^4/RT)$	L mol^{-1} s^{-1}	(Kalfas et al., 1993)
k_{tc}^0	$9.8 \times 10^7\exp(-701/RT)$	L mol^{-1} s^{-1}	(E. H. Hukkanen, 2004)
k_p^0	$4.92 \times 10^5\exp(-4353/RT)$	L mol^{-1} s^{-1}	(E. H. Hukkanen, 2004)
ρ_m	$968.0 - 1.15(T - 273.15)$	g L^{-1}	(Hoppe & Renken, 1998)
ρ_{poly}	$1212.0 - 0.845(T - 273.15)$	g L^{-1}	(Hoppe & Renken, 1998)
$M_{w,\ m}$	100.12	g mol^{-1}	–
$M_{w,\ I}$	232.12	g mol^{-1}	–
R	1.987	cal mol^{-1} K^{-1}	–

2nd moment for dead polymer

$$\frac{\partial \mu_2}{\partial t} = k_{tc}\left(\lambda_0\lambda_2 + \lambda_1^2\right) - \frac{\varepsilon_{poly}\mu_2}{1+\varepsilon_{poly}x}\frac{\partial x}{\partial t} \tag{45}$$

The monomer concentration is calculated with ε_{poly} and x defined in Eqs. (25) and (39):

$$[M] = \frac{[M_0](1-x)}{1+\varepsilon_{poly}x} \tag{46}$$

Using the moments calculated from Eqs. (40) ~ (45), the number-averaged molecular weight $\bar{M}_n$, mass-averaged molecular weight $\bar{M}_m$, and polydispersity index PD can be calculated as

$$\bar{M}_n = M_w\frac{\lambda_1+\mu_1}{\lambda_0+\mu_0} \tag{47}$$

$$\bar{M}_m = M_w\frac{\lambda_2+\mu_2}{\lambda_1+\mu_1} \tag{48}$$

$$PD = \frac{\bar{M}_m}{\bar{M}_n} \tag{49}$$

3.3. Kernels for PMMA particles

The particle growth rate by free radical polymerization is described by

$$G(x,T) = \varepsilon_{poly}\frac{L_0}{3}\frac{dx}{dt} \tag{50}$$

where L_0 is the initial diameter of a particle, $\frac{dx}{dt}$ means the monomer conversion change with time as represented in Eq. (39).

The kernel kinetics can be dominated by breakage in a small mixer with no coalescence observed. The kernel parameters of breakage-dominated PBEs have been reported as (E. H. Hukkanen, 2004)

$$B\left(N_j,T\right) = \int_j^\infty \beta\left(N_j,r\right)b(r)\upsilon(r)N_j\ dr \tag{51}$$

$$D\left(N_j,T\right) = b\left(N_j\right)N_j \tag{52}$$

$$\beta\left(N_j,r\right) \equiv \beta(L,r) = \frac{2.4}{r^3}\exp\left[-4.5\frac{\left(2L^3-r^3\right)^2}{r^3}\right] \tag{53}$$

$$b(r) = \frac{k_b}{(1+\theta_p)L^{2/3}}\exp\left[-\frac{a_b\sigma(1+\theta_p)^2}{\rho_p L^{5/3}\epsilon^{2/3}}\right] \tag{54}$$

$$\upsilon(r) = 2.0 \tag{55}$$

where k_b is the breakage frequency parameter, a_b is the breakage efficiency parameter associated with surface tension, σ (=0.013 N/m) is the surface tension at the monomer/polymer-water-surfactant interface, and ϵ is the turbulence energy dissipation rate.

Table 2
Empirical constants in the breakage rate functions

Proposed by	k_b	a_b
Hukkanen (E. H. Hukkanen, 2004)	0.13425	0.1728
Hsia (Hsia, 1981)	0.01031	0.06354

Table 3
Operating conditions for the case study.

Variable	Value	Unit
Inlet volume flowrate	5.5431e-7	m^3/s
Inlet mass fraction of particles	0.1	–
Inlet mass fraction of water	0.9	–
Initial concentration of monomer in particle	799.03	mol/m^3
Initial concentration of initiator in particles	3.303	mol/m^3
Initial mean diameter of particles in a parcel	80, 180	μm
Temperature	323.15, 363.15	K
RPM (down pumping)	350	rpm

For liquid-liquid dispersion, the breakage of liquid particles is affected by the turbulence energy dissipation. According to Kolmogorov's theory, the isotropic turbulence energy dissipation rate in a stirred reactor is determined by the design parameters of the reactor such as the reactor volume, the diameter of the impeller, and the revolutions per minute (RPM) as (Coulaloglou & Tavlarides, 1977)

$$\epsilon = \frac{\omega^3 D_I^3}{V_t} \tag{56}$$

However, this ϵ cannot express the spatial characteristics in the stirred tank reactor, since the Eq. (56) represents the averaged turbulence energy in the system. Therefore, the Reynolds average Navier-Stokes (RANS) modeling method which reflects the pressure drop is a good choice, in representing the local turbulence energy due to the flow. In the case-study, the Eq. (56) and empirical constants of (E. H. Hukkanen, 2004) are applied with the PBE only for the purpose of validating the model. The RANS model and the empirical parameters of (Hsia, 1981) are used for a reactor analysis. Table 2 lists the constant values for the breakage rate.

4. Process description

4.1. Reactor design and operating conditions

Fig. 2 represents the design and structure of the stationary CSTR used in the verification simulation. The CSTR is a round bottom cylindrical tank with a volume of 0.001 m^3 and the 45° pitched bladed down-pumping impeller with a diameter of 0.05 m. Roudsari et al. (Roudsari et al., 2013) designed this reactor to carry out various polymerization case studies (Roudsari et al., 2015; Xie & Luo, 2017). The operating conditions were set to maintain the residence time of 1800 seconds using the data from (E. H. Hukkanen, 2004) as shown in Table 3. Particularly, the temperature

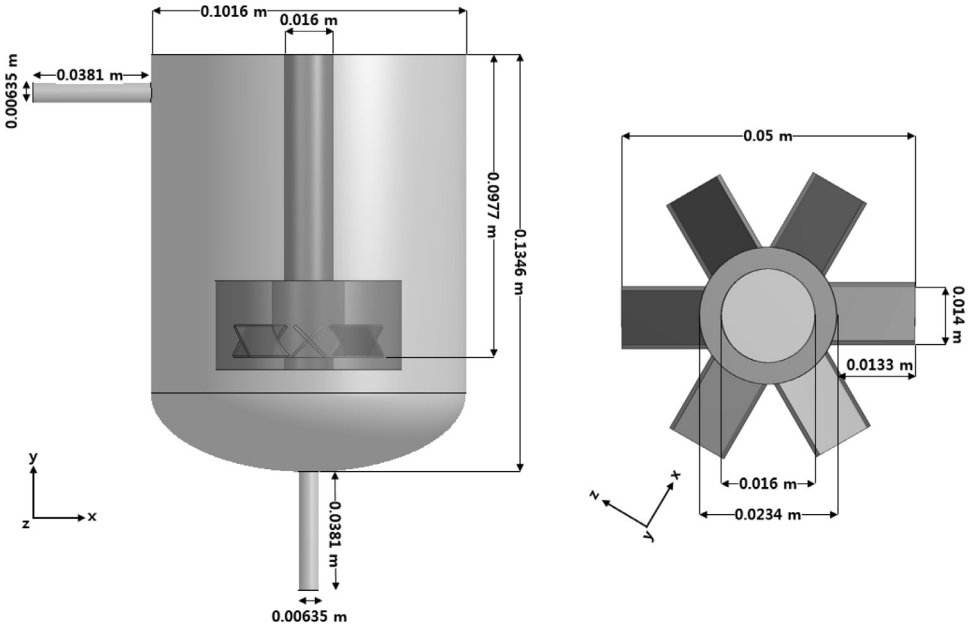

Fig. 2. Design of the CSTR.

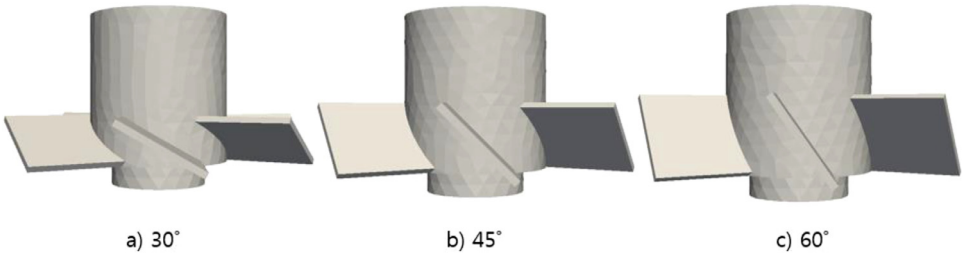

Fig. 3. Impeller designs of different blade angles.

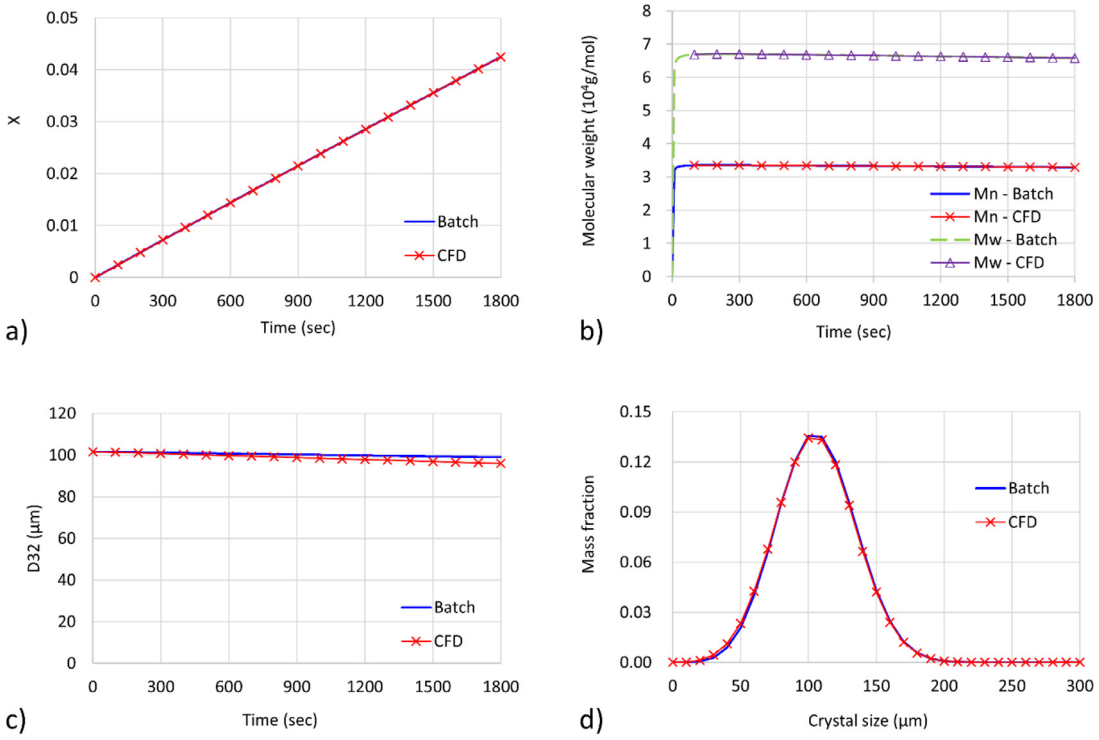

Fig. 4. Comparison of the CFD and well-mixed batch reactor simulations: a) Monomer conversion, b) Molecular weight of the polymer, c) Mean diameter of particles, d) Mass-weighted-average PSD at 1800 seconds

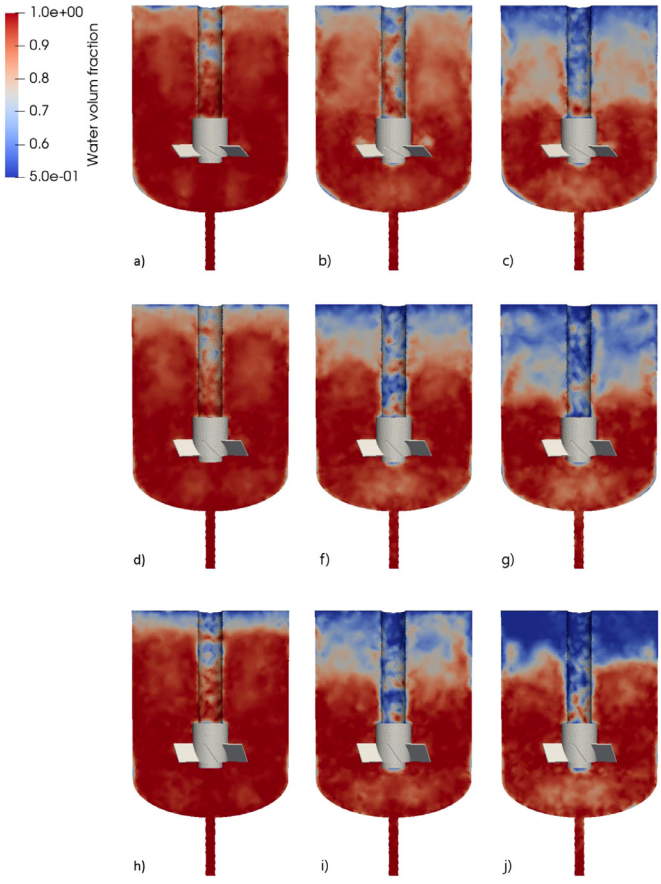

Fig. 5. Solvent volume fraction with different blade angles: a) 30° at 600 seconds, b) 30° at 1200 seconds, c) 30° at 1800 seconds, d) 45° at 600 seconds, f) 45° at 1200 seconds, g) 45° at 1800 seconds, h) 60° at 600 seconds, i) 60° at 1200 seconds, and j) 60° at 1800 seconds.

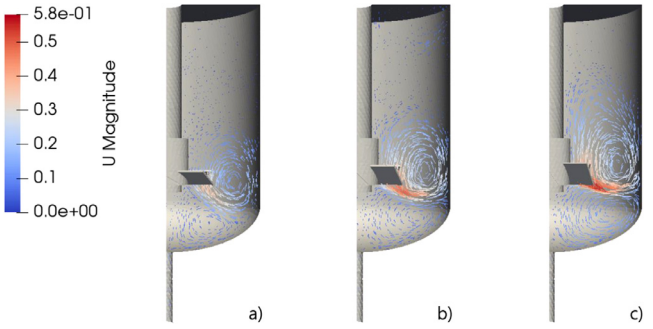

Fig. 6. Velocity of continuous phase at 1800 seconds: a) 30°, b) 45°, and c) 60°

is assumed to be controlled at a constant value. In the verification simulation, a stable polymer polymerization process is simulated at a temperature of 323.15 K, and in the case study, extreme polymerization is simulated at a temperature of 363.15 K. The initial particle size distribution is described by

$$N_j = \frac{1}{\sigma_s\sqrt{2\pi}}\exp\left[-\frac{1}{2\sigma_s{}^2}\left(D_j - D_0\right)^2\right] \tag{57}$$

where D_j is the particle diameter (μm), D_0 is the initial mean diameter of particles and $\sigma_s{}^2$ is the variance of 1000.

Through the case study, the relationship between the blade angle of the impeller and particle breakage is analyzed with the benefit of CFD simulation, which can incorporate 3D turbulence models such as the RANS model and can predict particle size changes based on the PBE. The case study compares the simulation results

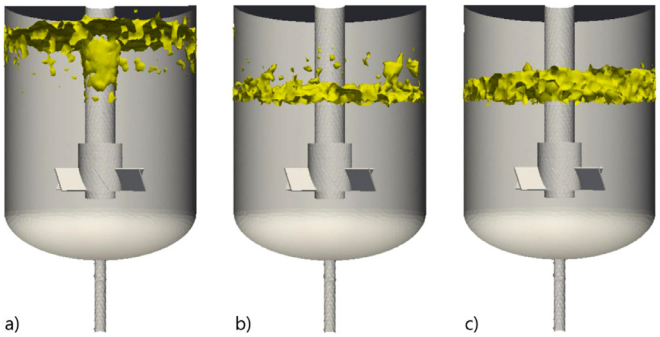

Fig. 7. Iso-surface of continuous phase of volume fraction 0.9 with time: a) 600 seconds, b) 1200 seconds, and c) 1800 seconds

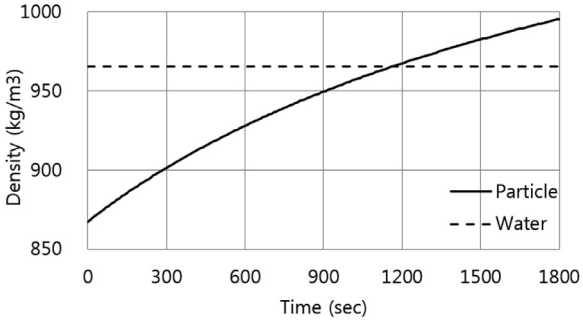

Fig. 8. Density of materials in the reactor over time

for a large angle of 60° and a smaller angle of 30° based on an angle 45 ° of the blade as shown in Fig. 3. The simulations predict time transient behavior for a period of 1800 seconds.

4.2. CFD model implementation

Regarding the numerical solution method, details of the MP-PIC-PBE algorithm can be found in Kim et al. Kim et al., 2020). The CFD model is developed on OpenFOAM 7.0. The technical details about the software and a tutorial can be found online (https://github.com/KAIST-LENSE/mppicPbePolyFoam). In addition, various CFD techniques were added to the MP-PIC-PBE method in simulating a highly nonlinear suspension polymerization reactor. The rotating motion of the impeller is set up using the multiple reference frame (MRF) method, which is an advanced version of the moving reference frame method. The MRF method divides the computational domain into stationary and moving domains and applies rotating motion to the moving domain. Appropriate acceleration terms are added to the fluid equations for the moving domain (Luo et al., 1994). Turbulent energy modeling is applied to the SST k-omega model, which is a hybrid method that combines the Wilcox k-omega model and the k-epsilon model (Menter, 1994). This method uses a blend function to activate the k-omega model at the wall and the k-epsilon model in the flow domain. The k-omega model is suited for computing flows in viscous sub-layers, and the k-epsilon model is ideal for predicting regions far from the wall. The energy equation is dropped by assuming that the temperature inside the tank is constant. Drag force and lift force are implemented between the particle phase and the carrier phase as described in Eqs (6) and (7). The computational domains are drawn in full 3D, and the mesh comprises around 250,000 cells in total. All CFD simulations have been performed on 22 cores of Intel (R) CPU of E5-2699 v4. The simulation time has been about 7 days for a physical time duration of 1800 seconds using the time step size of 0.001 to 0.05 seconds and keeping the Courant-Friedrichs-Lewy condition of 0.5.

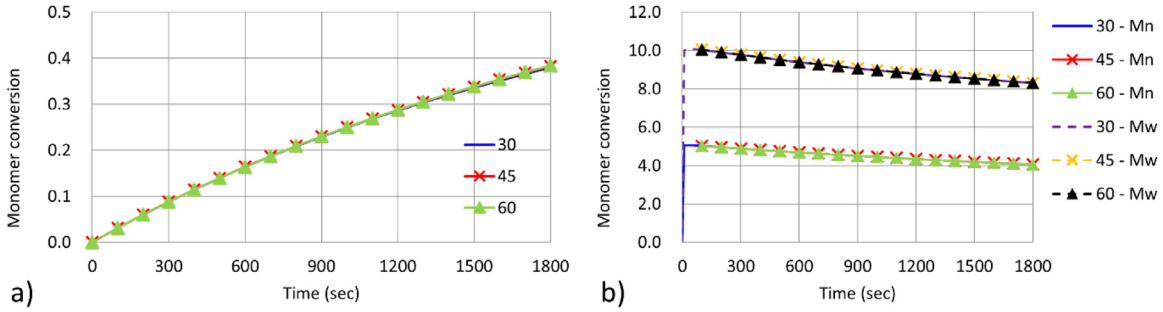

Fig. 9. Polymer properties in the tank over time: a) Average monomer conversion, b) Number and weight averaged molecular weight.

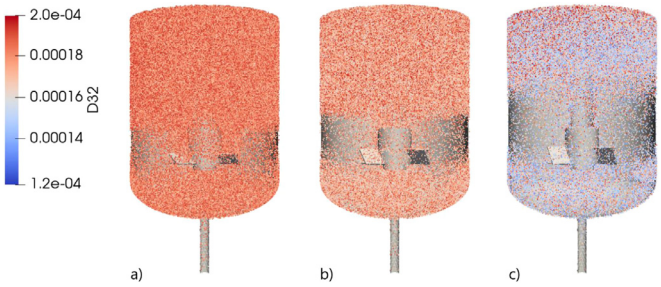

Fig. 10. Mean diameter of parcels at 1800 seconds: a) 30°, b) 45°, and c) 60°.

5. Result analysis

5.1. Validation of MP-PIC-PBE for suspension polymerization

Since the inside of the parcel is assumed to be perfectly mixed, it exhibits the identical reaction kinetics as a well-mixed batch reactor with a constant temperature, although it has complex movements in a reactor. Therefore, the CFD simulation with the perspective of the oldest parcel inside the reactor was compared to the simulation of a well-mixed batch reactor to verify the numerical accuracy of the MP-PIC-PBE method for polymerization. The mathematical model for the batch reactor was referred from Hukkanen (E. H. Hukkanen, 2004), where the model and parameters for the polymerization and PBE kernels were validated through comparison of the results from experiment and simulation (E. H. Hukkanen, 2004). As shown in Fig. 4, the results of the MP-PIC-PBE simulation show identical behavior to the results of the reference. At 1800 seconds, the monomer conversion to polymer is 0.04249 in the CFD simulation and 0.04250 in the well-mixed batch reactor simulation. The number average molecular weight and mass average molecular weight are 329,051 and 658,084 in the CFD simulation, compared to 329,046 and 658,069 g/mol in the batch reactor simulation. The mean diameter of particles reduces to 95.95 in the CFD and 98.92 μm in the batch reactor simulation.

5.2. Analysis of blade angle effects

The mixing efficiency is analyzed for different blade angles. MMA is a monomer that has a lower density than the solvent of water. Thus, as shown in Fig. 5, the injected particles, which are a mixture of monomer (MMA) and initiator (BPO), accumulate over a period of time near the reactor top by lift force. Even though the density difference leads to distinct solute and solvent regions in all the cases, the low blade angle intensifies the down pumping and mixing effect between the particles and water. Fig. 6 represents why a lower the blade angle leads to a more efficient pumping effect (Tsui et al., 2006). For the low blade angle of 30°, the direction of the down flow of the solvent gets closer to the floor. Therefore, the strong drag force between the particles and the solvent causes the particles to move from top to bottom of the reactor and induces good mixing. In addition, the upward flow near the walls may also affect the mixing effect, and Fig. 6 a) indicates that the drag force for the upward direction is decreased with the low blade angle. However, the lift force (buoyancy) continuously transfers the particles to the top of the reactor. In the PMMA suspension polymerization, since the down-pumping is more important than the up-pumping, the moderately low blade angle turns out to be more efficient for mixing overall.

Fig. 7 indicates the iso-surface of water volume fraction 0.9 regarding Fig. 5 h)-j). Fig. 7 a) and b) represent that the particle layer increases over time, but Fig. 7 c) shows that the layer does not increase. According to this result, it can be explained that the mixing of the system has entered a plateau after about 1200 seconds.

Fig. 8 explains how the mixing of the system is rapidly stabilized. The density of particles in the reactor increases over time by polymerization. As a result, the average density of particles exceeds that of water at about 1160 seconds. From the moment the density is reversed, the effect of lift disappears. As the particle density increases, the downward flow due to the gravity increases and the mixing rate of the system increases rapidly.

Under the assumption of well-mixed, the resulting polymer properties are nearly the same for all the different blade angles because the injected particles accumulate at the top of the reactor for 1800 seconds. As shown in Fig. 9, the monomer conversion at 1800 seconds is calculated as 0.380 at 30°, 0.383 at 45°, and 0.384 at 60°, showing very little difference. Though the difference in conversion is small, we observe that the lower the angle, the greater the influence of the down pumping flow, causing the particles to be ejected to the bottom of the reactor, thus reducing the overall residence time of the particles. The polydispersity index at 1800 seconds is predicted to be about 2.045 at all angles.

Regarding particle breakage, the higher blade angle breaks down the particles into smaller particles, as shown in Fig. 10. The minimum mean diameter of parcels is calculated as 155.3 at 30°, 146.2 at 45°, and 118.1 μm at 60°. The average mean diameter of particles is predicted as 181.7 at 30°, 175.9 at 45°, and 164.5 μm at 60°. At a same RPM, the difference in the turbulence dissipation rate is the main reason why a higher blade angle breaks the particles into smaller size. Fig. 11 shows that the high blade angle increases the turbulence dissipation rate around the impeller, and widens the range of generating and dissipating turbulence energy in the reactor (see Fig. 12). As a result, the maximum value of the turbulence energy dissipation rate is observed as 0.709 at 30°, 0.945 at 45°, and 1.414 m^2/s^3 at 60°.

In Figs. 7 and 8, the correlation between the change in particle density due to polymer growth and the mixing effect in the tank was explained. In addition, Fig. 13 demonstrates the effect of the particle density change on the particle size. The impeller, which had initially been stopped, started to rotate to induce par-

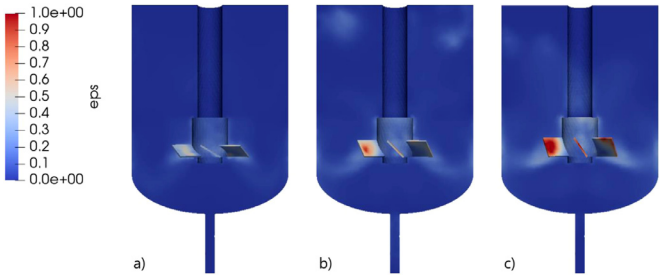

Fig. 11. Turbulence energy dissipation rate profiles at 1800 seconds: a) 20°, b) 45°, and c) 60°.

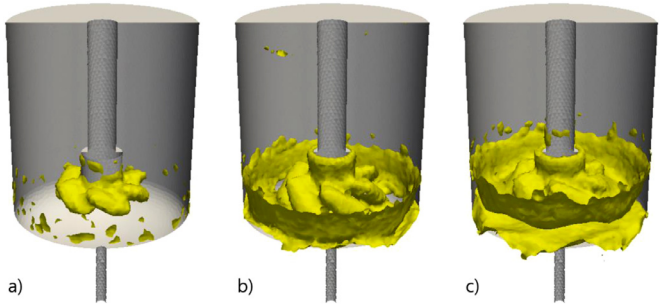

Fig. 12. Isosurface of continuous phase of turbulence dissipation rate 0.1 m^2/s^3 at 1800 seconds: a) 20°, b) 45°, and c) 60°.

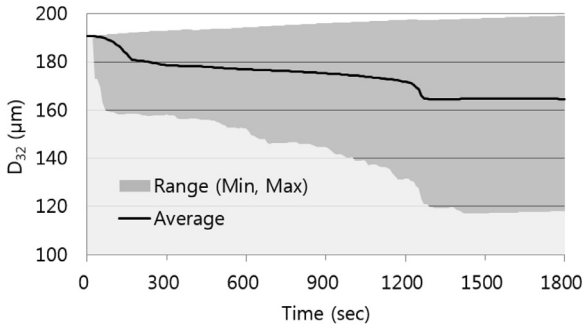

Fig. 13. Average mean diameter of parcels in the tank over time.

ticle breakage. And then, at about 150 seconds, the flow pattern is stabilized and the breakage rate becomes soft. Particularly, after about 1160 seconds, a decrease in the average size of the particles is observed for about 100 seconds. With the average particle size reduction, the minimum particle size is also decreased, which means that rapid mixing due to the particle density change affects the turbulence energy in the reactor. Finally, after about 1260 seconds, the particle size remains constant and the system is stabilized.

6. Conclusion

This study is the first to analyze the transport phenomena occurring in suspension polymerization using the MP-PIC-PBE method. In particular, the particle flow predicted by the Lagrangian frame clearly shows the suspension flow patterns induced by drag and lift forces. Moreover, the case study confirms the interaction between the blade angle of the impeller and the particle size of resin in the CSTR.

According to the simulation results, a low blade angle induces the down pumping of the particles, thus increasing the mixing efficiency. On the other hand, the high blade angle widens and intensifies the region and rate of turbulence dissipation in the reactor, breaking down the particles to smaller sizes. Therefore, in the case of suspension polymerization with the monomer of a lower density than the continuous phase, an appropriately chosen blade angle can increase the mixing effect. On the other hand, if stakeholders want to get smaller particles, replacing the impeller with one with a high blade angle will be a good strategy. However, this change can worsen the mixing effect and increased the variance of particle size distribution at the same time.

The simulation results suggest that the solute density exceeds the solvent density due to polymer growth, resulting in a rollover phenomenon between the two phases. And this roll-over phenomenon speeds up the mixing in the tank and accelerates the system stabilization. However, the case study was simulated in a small reactor measuring 0.001 m^3 in volume. It's difficult to say how the rollover will affect commercial size systems. In particular, the analyzed system has been assumed to be isothermal and does not reflect the temperature change due to the rollover phenomenon. This dynamic change in the flow can significantly affect the system temperature in a large-size system, despite the presence of temperature control through a jacket. Therefore, our next step is to study the control of commercial-scale processes with the help of the CFD model. For this, the CFD model will be updated to represent the heat transfer phenomenon inside the reactor with an outer cooling jacket.

Author Contribution Statement

Shin Hyuk Kim: Conceptualization, Methodology, Software, Writing - Original Draft. Jay H. Lee: Supervision, Writing - Review & Editing. Richard D. Braatz: Conceptualization, Writing - Review & Editing

Declaration of Competing Interest

The authors declare that they have no known competing financial interests or personal relationships that could have appeared to influence the work reported in this paper.

Acknowledgement

This work was supported by the National Research Foundation of Korea(NRF) grant funded by the Korea Government(MSIT) (No. 2021R1C1C2012717).

References

Barkanyi, A., Nemeth, S., 2015. Stochastic Simulation of Droplet Interactions in Suspension Polymerization of Vinyl Chloride. Periodica Polytechnica-Chem. Eng. 59, 129–137.
Barkanyi, A., Nemeth, S., Lakatos, B.G., 2013. Modelling and simulation of suspension polymerization of vinyl chloride via population balance model. Comput. Chem. Eng. 59, 211–218.
Coulaloglou, C.A., Tavlarides, L.L., 1977. Description of interaction processes in agitated liquid-liquid dispersions. Chem. Eng. Sci. 32, 1289–1297.
Crowley, T.J., Choi, K.Y., 1998. Experimental studies on optimal molecular weight distribution control in a batch-free radical polymerization process. Chem. Eng. Sci. 53, 2769–2790.
Dowding, P.J., Vincent, B., 2000. Suspension polymerisation to form polymer beads. Colloids Surf. A 161, 259–269.
Ghosh, P., Gupta, S.K., Saraf, D.N., 1998. An experimental study on bulk and solution polymerization of methyl methacrylate with responses to step changes in temperature. Chem. Eng. J. 70, 25–35.
Hoppe, S., Renken, A., 1998. Modelling of the free radical polymerisation of methylmethacrylate up to high temperature. Polym. React. Eng. 6, 1–39.
Hsia, M.A., 1981. The modeling of liquid–liquid extraction in stirred tanks by a simulation approach (Doctoral dissertation). Illinois Institute of Technology, Chicago, Illinois.
Hukkanen, E.H., 2004. A systems approach to the modeling and control of molecular, microparticle, and biological distribuitons (Doctoral dissertation). University of Illinois at Urbana-Champaign, Chicago, Illinois.
Hukkanen, E.J., Braatz, R.D., 2005a. Identification of particle-particle interactions in suspension polymerization reactors. In: ACC: Proceedings of the 2005 American Control Conference, 1-7, pp. 925–930 Vols.

Hukkanen, E.J., Braatz, R.D., 2005b. Worst-case and distributional robustness analysis of the full molecular weight distribution during free radical bulk polymerization. In: ACC: Proceedings of the 2005 American Control Conference, 1-7, pp. 3115–3120 Vols.
In: (eds) In Hukkanen, E.J., VanAntwerp, J.G., Braatz, R.D., 2007. Identification and Control of Polymerization Reactors. In: Sánchez Peña, R.S., Cayuela, V.P., Casín, J.Q. (Eds.), Identification and Control. Springer-Verlag, London, pp. 3–41.
Hungenberg, K.D., Wulkow, M., 2018. Phases and Phase Transitions. Model. Simul. Polym. Reaction Eng. 163–191.
Kalfas, G., Ray, W.H., 1993. Modeling and Experimental Studies of Aqueous Suspension Polymerization Processes .1. Modeling and Simulations. Ind. Eng. Chem. Res. 32, 1822–1830.
Kalfas, G., Yuan, H., Ray, W.H., 1993. Modeling and Experimental Studies of Aqueous Suspension Polymerization Processes .2. Experiments in Batch Reactors. Ind. Eng. Chem. Res. 32, 1831–1838.
Kim, S.H., Lee, J.H., Braatz, R.D., 2020. Multi-phase particle-in-cell coupled with population balance equation (MP-PIC-PBE) method for multiscale computational fluid dynamics simulation. Comput. Chem. Eng. 134, 106686.
Lin, C.C., Wang, Y.F., 1981. Suspension Polymerization of Methyl-Methacrylate .1. Modeling of Reaction-Kinetics. J. Appl. Polym. Sci. 26, 3909–3915.
Luo, J.Y., Issa, R.I., Gosman, A.D., 1994. Prediction of Impeller Induced Flows in Mixing Vessels Using Multiple Frames of Reference. In: Eighth European Conference on Mixing, pp. 549–556.
Menter, F.R., 1994. Two-equation eddy-viscosity turbulence models for engineering applications. AIAA J. 32, 1598–1605.
O'Neil, G.A., Wisnudel, M.B., Torkelson, J.M., 1998. An Evaluation of Free Volume Approaches to Describe the Gel Effect in Free Radical Polymerization. Macromolecules 31, 4537–4545.
Okullo, A., Tibasiima, N., Barasa, J., 2017. Modeling and Simulation of an Isothermal Suspension Polymerization Reactor for PMMA Production Using Python. Adv. Chem. Eng. Sci. 7, 408–419.
Ramkrishna, D., 2000. Population balances: theory and applications to particulate systems in engineering. Academic Press, San Diego, CA.
Razmi, H., Goharrizi, A.S., Mohebbi, A., 2019. CFD simulation of an industrial hydrocyclone based on multiphase particle in cell (MPPIC) method. Sep. Purif. Technol. 209, 851–862.
Rigopoulos, S., 2010. Population balance modelling of polydispersed particles in reactive flows. Prog. Energy Combust. Sci. 36, 412–443.
Roudsari, S.F., Dhib, R., Ein-Mozaffari, F., 2015. Mixing Effect on Emulsion Polymerization in a Batch Reactor. Polym. Eng. Sci. 55, 945–956.
Roudsari, S.F., Ein-Mozaffari, F., Dhib, R., 2013. Use of CFD in modeling MMA solution polymerization in a CSTR. Chem. Eng. J. 219, 429–442.
Snider, D.M., 2001. An incompressible three-dimensional multiphase particle-in-cell model for dense particle flows. J. Comput. Phys. 170, 523–549.
Snider, D. M., O'Rourke, P. J., & Andrews, M. J., 1997. An Incompressible Two-Dimensional Multiphase Particle-in-Cell Model for Dense Particle Flows.
Thapa, R.K., Frohner, A., Tondl, G., Pfeifer, C., Halvorsen, B.M., 2016. Circulating fluidized bed combustion reactor: Computational Particle Fluid Dynamic model validation and gas feed position optimization. Comput. Chem. Eng. 92, 180–188.
Tsui, Y.-Y., Chou, J.-R., Hu, Y.-C., 2006. Blade Angle Effects on the Flow in a Tank Agitated by the Pitched-Blade Turbine. J. Fluids Eng. 128, 774–782.
Xie, L., Luo, Z.H., 2017. Multiscale Computational Fluid Dynamics-Population Balance Model Coupled System of Atom Transfer Radical Suspension Polymerization in Stirred Tank Reactors. Ind. Eng. Chem. Res. 56, 4690–4702.
Zhang, S.X., Ray, W.H., 1997. Modeling and experimental studies of aqueous suspension polymerization processes .3. Mass-transfer and monomer solubility effects. Ind. Eng. Chem. Res. 36, 1310–1321.